phys. stat. sol. (b) **245**, No. 3, 502–510 (2008) / **DOI** 10.1002/pssb.200777703

physica status solidi b
www.pss-b.com
basic solid state physics

On the atomic level deformations in the auxetic zeolite natrolite

Ruben Gatt, Victor Zammit, Christian Caruana, and Joseph N. Grima*

Department of Chemistry, University of Malta, Msida MSD 2080, Malta

Received 15 May 2007, revised 5 December 2007, accepted 8 December 2007
Published online 12 February 2008

PACS 62.20.–x, 81.05.Zx

* Corresponding author: e-mail joseph.grima@um.edu.mt

Auxetics (i.e. systems with negative Poisson's ratios) exhibit the unexpected feature of becoming fatter when stretched and narrower when compressed. A particular class of materials which has attracted significant attention in recent years in view of its potential for auxeticity is that of zeolites, in particular, the zeolite NAT where auxeticity has now been experimentally measured. Here we use molecular modelling to accurately reproduce through force-field based simulations the experimentally measured negative Poisson's ratios in NAT. We also simulate and measure the atomic level deformations that result when NAT is mechanically deformed and use these to evaluate whether existing models can be used to explain the negative Poisson's ratios in natrolite. In particular we show that existing 2D models involving 'rotating semi-rigid quadrilaterals' can explain some aspects of the behaviour of NAT and make suggestions how such models can be improved so as to provide a better description of NAT in the auxetic (001) plane.

1 Introduction Auxetics are systems (materials or structures) which exhibit the property of expanding laterally when uniaxially stretched, a term which is equivalent to saying that the system exhibits a negative Poisson's ratio [1]. Although auxetics are not commonly encountered in everyday applications, it is well known that they can exist, and in recent years various systems have been reported to exhibit negative Poisson's ratio [2–47]. These systems include various naturally occurring or man-made materials ranging from microstructured materials such as foams [10–15], microporous polymers [16–18] to molecular-level auxetics such as polymers [1, 19–23], metals [24], silicates [25–33, 37] and zeolites [34, 35, 43–46, 55]. All of these systems are characterised by having macro-, micro- or nanostructures with very particular geometric features that allow for auxetic behaviour when they deform through appropriate deformation mechanisms. In recent years, various models [10–15, 34, 35, 39–44, 47, 55], especially two-dimensional models which describe the behaviour of a particular cross-section of the material, have been developed in an attempt to explain the occurrence of negative Poisson's ratios. Such models can be extremely useful as they provide a better insight into the mechanisms by which negative Poisson's ratios can be achieved. It is important to note that despite the widespread use of two-dimensional models [35, 39–43, 55], these models can never fully represent all the deformations that are occurring in three dimensional auxetic structures or materials. Nevertheless, they are very valuable in providing researchers with a picture of the auxetic behaviour in the 2D plane where it is measured (the Poisson's ratio is a two dimensional property).

Also, most models derived so far represent highly idealised scenarios, whilst the behaviour of the real materials is much more complex. For example, whilst the 'rotating rigid polygons' model can explain the presence of the auxetic effect in various classes of materials, they overestimate the auxeticity and fail to predict the dependence of the Poisson's ratios on the direction of loading [32, 34]. This problem can be rectified (at least in part) through further development of the models to include concurrent deformation mechanisms which could be taking place when the real material is subjected to mechanical loads, for example by using semi-rigid polygons [44], or, by attempting to produce a more 3D detailed model which would be essential to understand the full 3D mechanism, possibly by extending existing 2D models.

A class of materials which in recent years has attracted considerable attention is that of auxetic zeolites [34, 35,

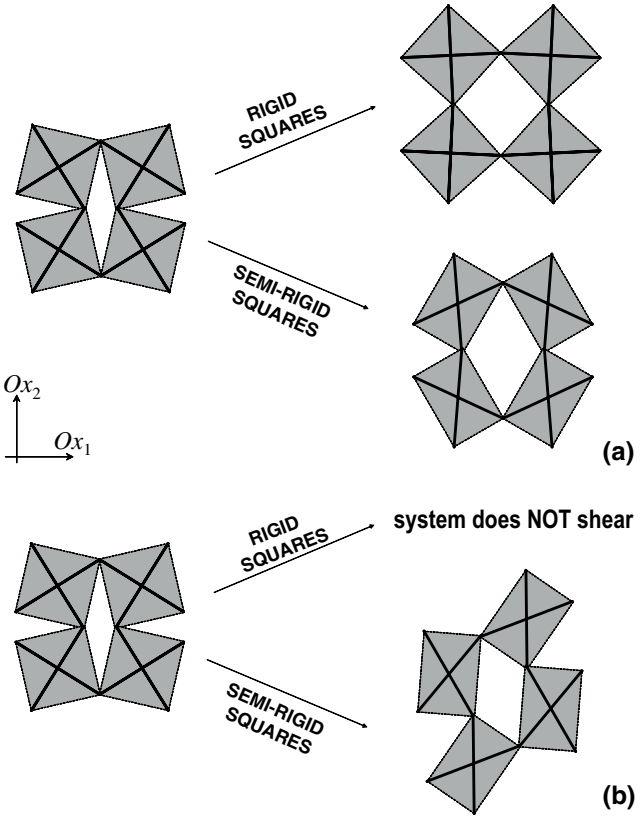

Figure 1 A comparison of the 'rotating rigid squares' [34, 40, 41] and the 'rotating semi-rigid squares' [44] models showing deformations as a result of (a) stretching in the Ox_2 direction, and (b) shearing.

43–46, 55]. The first report that various members of the zeolite class of materials could be auxetic was made in 1999, when it was reported that various zeolites (e.g. THO, NAT, EDI, JBW, etc.) were predicted to exhibit negative Poisson's ratio [34, 35]. Since this preliminary force-field based molecular modelling work, various studies have been conducted, both theoretical and experimental in an attempt to obtain a better understanding of these properties. These include a modelling study [35, 44] where the predicted negative Poisson's ratio in (001) plane of the SiO_2 equivalents of THO and related frameworks were explained by a model based on semi-rigid rotating squares (a variation of idealised rotating squares [34, 40, 41], (see Fig. 1) and a study which attempted to explain the behaviour of NAT in terms of parallelograms [55]. More significantly, there was an experimental study using the Brillouin light scattering technique which measured the full 6×6 stiffness matrix of NAT single crystals [45]. When these elastic constants are analysed [46], NAT is confirmed to exhibit negative Poisson's ratios. In fact, an analysis of the full set of experimental stiffness coefficients (c_{ij}) using standard axis transformation techniques [48], clearly indicates that NAT exhibits negative Poisson's ratios for loading in certain directions with maximum auxeticity of –0.12 being exhibited in the (001) plane for loading at ~45° to the major [100] and [010] directions [46].

Although the experimental verification of auxeticity in NAT, the first experimental verification of auxeticity in any zeolite, signifies an important development in the field of auxetic zeolites, the method used to measure the elastic constant does not provide information on the deformation mechanism which results in this behaviour. Nevertheless, the measured anisotropy in the experimentally determined Poisson's ratios in the (001) plane where maximum auxeticity is exhibited for loading is very significant since it is consistent with earlier preliminary molecular modelling work [34] on the hypothetical SiO_2 equivalent of the NAT which had predicted maximum auxeticity in the same directions. (The hypothetical SiO_2 equivalent of NAT is a modified version of natrolite where all the aluminium atoms are replaced by silicon atoms, with no extra-framework species present.) The predicted auxeticity in the (001) plane in the hypothetical SiO_2 equivalent of NAT, including the anisotropy, has been well explained using a 2D 'rotating semi-rigid squares' model [40, 41, 44] (see Fig. 1) which permitted the squares to become rectangles. However, the hypothetical SiO_2 equivalent of NAT is chemically different from the actual NAT and thus one would expect that the predictions made on the SiO_2 equivalent of NAT may not be fully applicable to NAT proper. In fact, the results that were obtained in the experimental study [45] on NAT, confirm the main trends observed in the earlier modelling studies on the hypothetical SiO_2 equivalent of NAT, but also showed some differences, most significantly, a decrease in the extent of auxeticity. Furthermore, in NAT, auxeticity was only exhibited for loading in certain directions in the (001), and not for loading in all direction as observed in the hypothetical SiO_2 equivalent of NAT.

In view of all this, in this paper we will attempt to obtain a better picture of the behaviour of NAT by first attempting to accurately reproduce through force-field based simulations the experimentally measured structure of NAT and the experimentally measured negative Poisson's ratios, and then simulate and measure the atomic level deformations that result when NAT is mechanically deformed. Furthermore, we compare the atomic level deformations in NAT to the ones in the hypothetical SiO_2 equivalent of NAT and in hypothetical NAT-type frameworks where the tetrahedra are assumed to be rigid. We also examine the suitability of existing models to explain the negative Poisson's ratios in natrolite on the basis of the simulated data.

2 Simulating the structure and mechanical properties of NAT In this study we performed simulations on NAT (i.e. $Na_2(Al_2Si_3O_{10})\cdot 2H_2O$, Fdd2 symmetry) using the software package Cerius^2 V4.2 (Accelrys Inc.) running on a SGI Octane2 workstation. The crystals were aligned in global *XYZ* space such that the [001] crystal direction is always parallel to the global *Z*-axes and the [010] crystal direction aligned the global *Y*,*Z*-plane. An energy expres-

Table 1 A comparison of the unit cell parameters of NAT as simulated by the Burchart-Universal force-field (NAT_CW) with the experimentally determined values (NAT_EXP) [43].

	NAT_EXP	NAT_CW	
		Burchart-Universal	CVFF
a (Å)	18.298	18.082	17.920
b (Å)	18.650	19.327	18.006
c (Å)	6.559	6.516	6.611
α, β, γ (°)	90.000	90.000	90.000

sion for each crystal was set up using the Burchart-Universal force-field, a force-field which has been used by other workers to simulate the properties of zeolites, e.g. in a study on the zeolite SSZ-48 [52]. (The Burchart-Universal force-field is a hybrid between the Burchart force-field [49], a zeolites specialised force-field used in our earlier preliminary study of the SiO_2 equivalent which provides the parameters for the framework and the Universal force-field [50] which provides the parameters for Na^+ and H_2O.) The partial charges were calculated using the Charge-Equilibration procedure developed by Rappe et al. where the charges on the $Na_2(Al_2Si_3O_{10})$ part of the system were calculated separately from those of the water molecules. A relative dielectric constant of 2.65 was used, this being the average of the dielectric constant suggested in the Burchart force-field (4.30) and the one assumed in the Charge-Equilibration method (1.00). All non-bond terms added using the Ewald summation technique [51].

The simulations were repeated using the protocol for modelling NAT identified by Williams et al. [55] which makes use of the CVFF force-field [53] with the charges being assigned as per the Dreiding-Universal force-field [54].

Geometry optimisations were performed to the default Cerius^2 high convergence criteria which include the requirement that the RMS force on each atom must be less than 0.001 kcal mol^{-1} Å^{-1}. No symmetry constraints were used in the minimisations (i.e. the systems were assumed to exhibit a P1 symmetry).

The resulting atomic configurations of the minimised conformations were found to be very similar to that measured experimentally [56] as shown in Tables 1 and 2. In fact, we found that the cell parameters as predicted by the two force-fields are remarkably close to those of the experimentally determined structure: the cell parameter a is slightly underestimated by the two force-fields (by around 1% for the Burchart-Universal force-field and *circa* double the amount for the CVFF force-field), the b cell parameter is overestimated and underestimated by the Burchart-Universal force-field and the CVFF force-field respectively by ~3.5% and the c cell parameter is underestimated and overestimated by the Burchart-Universal force-field and the CVFF force-field respectively by ~0.7%. The cell angles were all modelled correctly (with a value of 90°).

Also, when we analysed the Burchart-Universal and CVFF simulated forms of NAT in terms of the projected 'squares' in the (001) plane (or rather 'quadrilaterals'), see Table 3, we found that both force-fields can successfully replicate the observation that all the eight individual 'square units' ABCD in each unit cell of natrolite (see Fig. 2) are actually parallelograms of the same size, an observation which was also made by Willams et al. [55] who also identified parallelogramic units. This is very significant, particularly in view of the fact that the ABCD quadrilaterals in the hypothetical SiO_2 equivalents of the NAT frameworks are always predicted to be squares in the undeformed states.

Simulations suggest that both force-fields can reproduce the shape and size of the individual parallelograms ABCD fairly well. The CVFF force-field appears to be slightly better than the Burchart-Universal force-field for modelling the side lengths of the parallelograms, the inter-

Table 2 A comparison of the atomic positions for NAT (NAT_CW) as simulated by the Burchart-Universal force-field and by the CVFF force-field with the experimentally determined values (NAT_EXP) [56].

	NAT_EXP			NAT_CW					
				Burchart-Universal			CVFF		
	a	b	c	a	b	c	a	b	c
Si	0.000	0.000	0.000	0.000	0.000	-0.023	0.000	0.000	–0.004
Si	0.153	0.211	0.615	0.154	0.211	0.589	0.146	0.220	0.607
Al	0.039	0.095	0.601	0.042	0.089	0.589	0.029	0.101	0.603
O	0.022	0.069	0.868	0.036	0.058	0.836	0.019	0.070	0.855
O	0.070	0.181	0.604	0.075	0.174	0.587	0.061	0.194	0.600
O	0.098	0.036	0.491	0.100	0.035	0.451	0.097	0.046	0.479
O	0.207	0.155	0.718	0.207	0.162	0.722	0.193	0.157	0.722
O	0.179	0.227	0.389	0.186	0.218	0.365	0.179	0.230	0.383
Na	0.219	0.033	0.611	0.193	0.039	0.718	0.213	0.037	0.603
O	0.057	0.188	0.117	0.019	0.186	0.138	0.058	0.198	0.111
H	0.051	0.148	0.017	–0.020	0.162	0.060	0.060	0.147	0.058
H	0.090	0.188	0.161	0.057	0.150	0.161	0.108	0.201	0.175

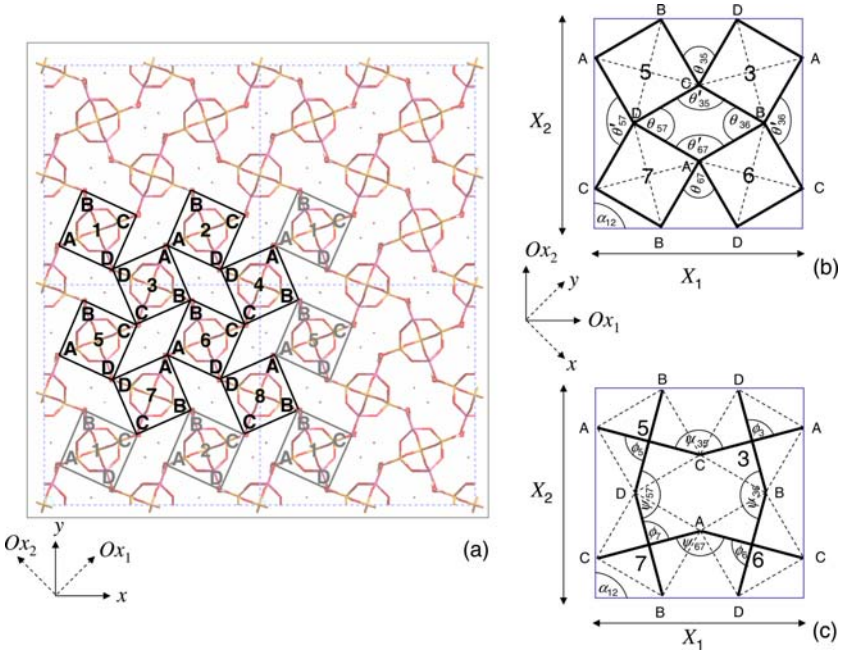

Figure 2 (online colour at: www.pss-b.com) Definition of the variables monitored defined relative to NAT (shown in a), with (b) the squares shown in bold, representing the original 'rotating squares structure', and (c) the diagonals shown in bold, representing the new structure where the squares are replaced by their diagonals. This figure defines the parameters being used.

nal angles and the angles between the diagonals within the same parallelogram. For example, both force-fields correctly identified the smaller sets of internal angles in the parallelograms (ABC and CDA for parallelograms 1, 2, 5 and 6, and BCD and DAB for parallelograms 3, 4, 7 and 8) but the differences between the simulated angles and the equivalent ones for the experimentally measured structure are only ~0.5° in the case of the CVFF force-field compared to ~1° in the case of the Burchart-Universal force-field. It is interesting to note that although the lengths of the sides of the parallelograms as predicted by the CVFF force-field are slightly closer to the equivalent ones for the experimentally measured structure, and the CVFF force-field correctly predicts that sides AB and CD have a different length from BC and DA, the CVFF force-field fails to correctly identify the sides AB = CD as the longer sides and BC = AD as the shorter sides, a feature which is correctly modelled in the case of the Burchart-Universal force-field.

However, some considerable differences were observed in the measurements of the angles between the quadrilaterals. In fact, although both force-fields correctly predict that all the acute angles between the different parallelograms have the same magnitude (42.11° in the case of the experimentally determined structure) we find that the Burchart-Universal force-field overestimates this angle by ~5° whilst the CVFF force-field underestimates this angle by ~8°. Although these differences are quite significant, we note that the true value is approximately equal to the average of the two measurements as predicted by the different force-fields (average = 40.47°), i.e., the true picture of the behaviour of NAT is likely to be well represented by the average behaviour as simulated by these two force-fields.

Having ascertained that the simulated NAT structures compare well to the experimentally determined NAT, we proceeded with the simulations of the elastic constants from the second derivatives of the energy expressions from which the Poisson's ratios in the (001) plane (i.e. the plane where maximum auxetic behaviour was observed) were calculated using standard axis transformation techniques [48]. For both force-fields, the simulated off-axis profiles of the Poisson's ratios were found to be very similar to that measured experimentally as illustrated in Fig. 3, although the Burchart-Universal force-field predicted slightly better results.

We also performed analogous simulations on the all-silica (SiO_2) version of the NAT framework (henceforth referred to as NAT_SI) were all force-field parameters were taken from the Burchart and the CVFF force-field [48] so as to be able to compare the properties of the real zeolite with those of the hypothetical SiO_2 equivalent. As illustrated in Fig. 3, the two force-field once again agree with each other and with the earlier preliminary study [34] in finding the hypothetical NAT_SI significantly more auxetic than NAT_CW in the (001) plane with maximum auxeticity being exhibited for loading ~45° off-axis.

The good comparisons between the properties of NAT_CW as simulated by the two force-fields with the experimentally measured properties add confidence to the quality of the simulated results, and also suggest that the observed decrease in auxeticity of NAT_CW when compared to NAT_SI is due to the fact that the hypothetical SiO_2 equivalent of NAT is chemically different than NAT itself. In other words, when the predicted auxetic nature of the hypothetical SiO_2 equivalent of NAT is compared to NAT proper, the changes may be attributed primarily to differences in the in the composition and not to simulation errors.

Table 3 A description of the 2D projection of NAT in the (001) plane in terms of the 'rotating quadrilaterals' model. The parameters measured are defined in Fig. 2. (Grp I: [mn = 23, 14, 35, 46, 67, 58, 17, 28], Grp II: [mn = 13, 24, 36, 45, 57, 68, 27, 18]).

	data relating to individual quadrilaterals											angles between two quadrilaterals (degrees)			
	lengths (in Å)						angles (in degrees)								
	n	A_nB_n	B_nC_n	C_nD_n	D_nA_n	A_nC_n	B_nD_n	$A_nB_nC_n$	$B_nC_nD_n$	$C_nD_nA_n$	$D_nA_nB_n$	ϕ_n	mn	θ_{mn}	θ'_{mn}	Ψ_{mn}
NAT	1, 2, 5, 6	5.08	5.03	5.08	5.03	7.07	7.22	88.81	91.19	88.81	91.19	89.44	Grp I	42.11	137.89	132.12
EXP	3, 4, 7, 8	5.08	5.03	5.08	5.03	7.22	7.07	91.19	88.81	91.19	88.81	89.44	Grp II	42.11	137.89	132.12
NAT	1, 2, 5,6	5.15	4.90	5.15	4.90	6.97	7.24	87.76	92.24	87.76	92.24	87.07	Grp I	46.99	133.01	137.11
BU	3, 4, 7, 8	5.15	4.90	5.15	4.90	6.97	7.24	92.24	87.76	92.24	87.76	87.07	Grp II	46.99	133.01	137.11
NAT	1, 2, 5, 6	5.06	5.12	5.06	5.12	7.09	7.30	88.26	91.74	88.26	91.74	90.65	Grp I	33.95	146.05	123.93
CVFF	3, 4, 7, 8	5.06	5.12	5.06	5.12	7.09	7.30	91.74	88.26	91.74	88.26	90.65	Grp II	33.95	146.05	123.93

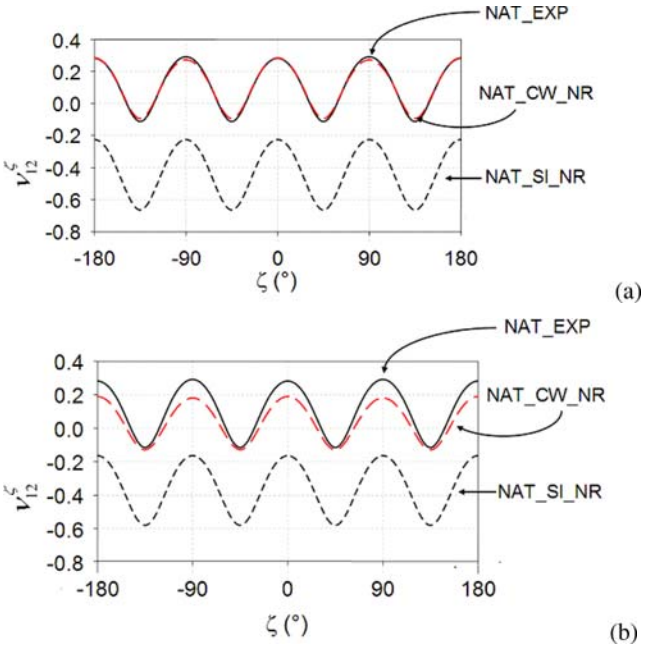

Figure 3 (online colour at: www.pss-b.com) A comparison of the Poisson's ratio in the (001) plane of NAT_EXP (i.e. using data for NAT as obtained experimentally), NAT_CW (i.e. using data for NAT with the cations and rigid water molecules as simulated by the Burchart-Universal force-field), NAT_SI (i.e. the SiO_2 equivalent of the empty NAT framework as simulated by the Burchart force-field), NAT_CW_R and NAT_SI_R (the equivalents of NAT_CW and NAT_SI respectively with the tetrahedra forced to remain rigid).

3 Simulating the deformation mechanism which results in auxetic behaviour in NAT In an attempt to understand more clearly the atomic-level deformations that take place when natrolite is mechanically loaded, we have performed force-field based simulations using the Burchart-Universal and CVFF force-fields (as described above) on NAT_CW where loads (in compression and shear) in the (001) plane were applied at 45° off-axis (to correspond with the directions of maximum auxeticity). In particular:

(a) For loading in compression, we applied loads which are 45° to the x-axis (a direction of maximum auxeticity), where the loads applied were:

$$\tilde{\boldsymbol{A}} = \frac{1}{2}\begin{pmatrix} \sigma & -\sigma & 0 \\ -\sigma & \sigma & 0 \\ 0 & 0 & 0 \end{pmatrix}, \quad (1)$$

$\sigma = -1.00\ \text{GPa}, -0.75\ \text{GPa}, \ldots, 0.00\ \text{GPa}$,

(b) For loading in shear the X,Y-plane, the loads applied were:

$$\tilde{\boldsymbol{A}} = \begin{pmatrix} \sigma & 0 & 0 \\ 0 & -\sigma & 0 \\ 0 & 0 & 0 \end{pmatrix}, \quad (2)$$

$\sigma = -0.20\ \text{GPa}, -0.15\ \text{GPa}, \ldots, 0.00\ \text{GPa}$.

Table 4 Gradients of plots of % changes (for lengths) and actual changes (for angles in degrees) vs. applied stress at 45° to the *y*-direction (in GPa) for NAT_SI. These values represent the change (percentage or actual) in the various lengths of sides/diagonals of squares etc. per 5% applied strain (= 0.05 × E_y^{45} GPa, where E_y^{45} is the simulated value of the Young's modulus E_y transformed through axis rotation about *z* of 45°. In the case of shear, the shear modulus G_{xy} substitutes for E_y). The parameters monitored are defined in Fig. 2. (Grp I: [*mn* = 23, 14, 35, 46, 67, 58, 17, 28], Grp II: [*mn* = 13, 24, 36, 45, 57, 68, 27, 18]).

		data relating to individual quadrilaterals											changes in angles between two quadrilaterals (degrees)			
		% change in lengths							changes in angles (angles in degrees)							
		n	A_nB_n	B_nC_n	C_nD_n	D_nA_n	A_nC_n	B_nD_n	$A_nB_nC_n$	$B_nC_nD_n$	$C_nD_nA_n$	$D_nA_nB_n$	φ_n	*mn*	θ_{mn}	θ'_{mn}	ψ_{mn}
(a) NAT_CW																
BU	stress	1, 2, 5, 6	0.14	1.91	0.14	1.91	–0.84	2.68	–2.02	2.02	–2.02	2.02	1.01	Grp I	3.58	–7.73	4.32
		3, 4, 7, 8	1.88	–1.13	1.88	–1.13	–1.33	2.38	–2.12	2.12	–2.12	2.12	–1.72	Grp II	7.73	–3.58	7.05
	shear	1, 2, 5, 6	–2.18	2.49	–2.18	2.49	0.25	–0.17	0.25	–0.25	0.25	–0.25	2.67	Grp I	–0.68	0.68	–0.80
		3, 4, 7, 8	–2.18	2.49	–2.18	2.49	–0.17	0.25	–0.25	0.25	–0.25	0.25	2.67	Grp II	–0.68	0.68	–0.80
CVFF	stress	1, 2, 5, 6	–0.49	2.30	–0.49	2.30	–0.50	2.25	–1.58	1.58	–1.58	1.58	1.60	Grp I	2.46	–5.51	2.20
		3, 4, 7, 8	2.54	–0.93	2.54	–0.93	–0.46	2.11	–1.47	1.47	–1.47	1.47	–1.99	Grp II	5.51	–2.46	5.79
	shear	1, 2, 5, 6	–2.27	2.09	–2.27	2.09	0.56	–0.66	0.70	–0.70	0.70	–0.70	2.50	Grp I	0.02	–0.02	–0.05
		3, 4, 7, 8	–2.27	2.09	–2.27	2.09	–0.66	0.56	–0.70	0.70	–0.70	0.70	2.50	Grp II	0.02	–0.02	–0.05
(b) NAT_SI																
BU	stress	1, 2, 5, 6	–0.12	0.75	–0.12	0.75	–0.35	0.97	–0.76	0.76	–0.76	0.76	0.50	Grp I	13.04	–14.55	13.27
		3, 4, 7, 8	0.79	–0.19	0.79	–0.19	–0.35	0.95	–0.75	0.75	–0.75	0.75	–0.56	Grp II	14.55	–13.04	14.33
	shear	1, 2, 5, 6	–2.41	2.46	–2.41	2.46	0.24	–0.21	0.26	–0.26	0.26	–0.26	2.79	Grp I	0.04	–0.04	0.04
		3, 4, 7, 8	–2.41	2.46	–2.41	2.46	–0.21	0.24	–0.26	0.26	–0.26	0.26	2.79	Grp II	0.04	–0.04	0.04
CVFF	stress	1, 2, 5, 6	–0.17	0.99	–0.17	0.99	–0.43	1.25	–0.96	0.96	–0.96	0.96	0.66	Grp I	12.01	–13.92	12.28
		3, 4, 7, 8	1.01	–0.23	1.01	–0.23	–0.44	1.21	–0.95	0.95	–0.95	0.95	–0.71	Grp II	13.92	–12.01	13.66
	shear	1, 2, 5, 6	–2.40	2.40	–2.40	2.40	0.27	–0.28	0.31	–0.31	0.31	–0.31	2.75	Grp I	0.10	–0.10	0.10
		3, 4, 7, 8	–2.40	2.40	–2.40	2.40	–0.28	0.27	–0.31	0.31	–0.31	0.31	2.75	Grp II	0.10	–0.10	0.10

We also performed analogous simulations on the all-silica (SiO_2) version of the NAT framework (NAT_SI) were all force-field parameters were taken from the Burchart and the CVFF force-field [48] so as to be able to compare the properties of the real zeolite with those of the hypothetical SiO_2 equivalent.

For each of the minimised system under an applied load, we measured various lengths and angles corresponding to the quadrilaterals ABCD identified in Fig. 2, and from these we extrapolated the change of these parameters (either as absolute values in the case of angles or as percentage changes in the case of lengths) per 5% applied strain. These results are listed in Table 4a for NAT_CW and in Table 4b for the hypothetical SiO_2 equivalent of NAT (NAT_SI).

The results for *uniaxial loading* shown in Table 4 suggest that NAT_CW and NAT_SI behave differently from each other. In particular, in the case of the NAT_CW, uniaxial loading at 45° to the *x*-direction will result in a significant changes in both the angles between the quadrilaterals ABCD and in the shape and size of the quadrilaterals ABCD, whilst in the case of NAT_SI, the changes are primarily concentrated in changes of the angles between the quadrilaterals ABCD whilst the changes in the shape and size of the quadrilaterals ABCD themselves are negligible.

For example, when the deformations are extrapolated to correspond to a 5% strain in the direction of loading, the CVFF force-field predicts that in the case of NAT_CW, there are changes in the angles between the squares or around 2.5°–5.5°; the internal angles of the quadrilaterals change by approximately 1.5°; the side lengths of the quadrilaterals ABCD change by up to ~2.5% whilst the diagonals behave in such a way that the diagonal AC decreases by about 0.5% whilst the diagonal BD increases by about 2%. In contrast to this, in the case of NAT_SI, the CVFF predicts that a 5% strain will result in approximately 12°–14° changes in the angles between the squares (i.e. ~3 times more than in NAT_CW) whilst the changes in the shape and size of the quadrilaterals ABCD for NAT_SI were consistently less than those observed in NAT_CW. The Burchart-Universal force-field predicts similar behaviour. All this suggests that the inclusion of the extra-framework Na^+ cations and H_2O molecules significantly lowers the ability of NAT (when compared to the NAT_SI) to mimic the behaviour of the idealised 'rotating quadrilaterals (squares)' model with the result that auxeticity is reduced. (The idealised model assumes deformations through rotation of the quadrilaterals without changes in the shape of these quadrilaterals.)

We also note that in all cases (i.e. for both NAT_CW and NAT_SI, and using both force-fields), the eight projected parallelograms ABCD in the unit cell do not remain all congruent to each other, and instead, four of these (no. 1, 2, 5 and 6) deform in one way and the other four (3, 4, 7 and 8) deform in a different way. Once again, this effect is much more visible in the case of NAT_CW than in the case of NAT_SI. In particular we note that both force-fields predict that at 5% extrapolated strain, the parallelograms 3, 4, 7 and 8 in NAT_CW are deforming in such a way that they lose the intensity of their parallelogramic character (i.e., becoming more rectangular) while the rest gain a stronger parallelogramic character in response to a positive stress. This is very significant because previous models have neglected to account for such phenomena. In particular, the model presented by Grima et al. [44] only permitted deformations where ABCD assume rectangular shapes[1] (the diagonals were assumed to be of constant length) whilst the more recent model presented by Williams et al. [55] assumes that all the ABCD parallelograms in the system remain congruent to each other.

Our simulations of *shear loading* suggest that NAT_CW and NAT_SI behave in a similar way when they are subjected to shear stresses applied at 45° to the *x*-direction. In fact, for both NAT_CW and NAT_SI, our simulations suggest that such a shear deformation will primarily result in changes in the angles between the diagonals, a property which in the case of NAT_SI results in the ABCD squares becoming rectangular (with the connectivity of the Type II rectangles as described by Grima et al. [57]). In fact, the CVFF simulations suggest that when the deformations are extrapolated to correspond to a 5% shear strain at 45° to the *x*-direction, one may observe that the angle ϕ between the diagonals changes by 2.5° in the case of NAT_CW and 2.75° in the case of NAT_SI whilst there is minimal change in the in the internal angles of the quadrilaterals ABCD which change by 0.7° in the case NAT_CW and ~0.3° in the case of NAT_SI. Furthermore in both cases, there is minimal change in the lengths of the diagonals. All this suggests that the presence of the extra-framework species has little effect on the deformation mechanism originating from applied shear stresses. This may be explained by the fact that the mode of deformation upon shearing primarily involves deformations of the quadrilaterals ABCD themselves and has little effect on the void region between the quadrilaterals (where the extra-framework Na^+ cations and H_2O molecules are contained).

Taking all this into consideration, one may conclude that the model described in Fig. 1 where the quadrilaterals ABCD (which are assumed to be initially squares) are represented by their diagonals which are connected at their centres though a joint with an associated stiffness k_ϕ whilst the diagonals of the different quadrilaterals are connected together through a hinge with associated stiffness k_ψ (see Figs. 1 and 2) can still describe some of the deformations observed in NAT_CW, particularly the deformations when the system is sheared, but it needs to be improved so as to enable a better description of the behaviour on uniaxial

[1] The model by Grima et al. [44] was developed primarily to explain the deformations in the hypothetical SiO_2 equivalents of the NAT framework, where the internal angles of the quadrilaterals ABCD deviate very little from 90°. In this respect, the model by Williams et al. [55] where the quadrilaterals ABCD are in the shape of parallelograms offers a significant improvement which is essential for the correct representation of the projection of NAT in the (001) plane.

loading. (The analytical model overestimates the extent of auxeticity, particularly in the case of NAT with the cations and water molecules [58]). In particular, this model should be extended to allow for changes in lengths of the diagonals, a feature which would permit the permitting the quadrilaterals to become parallelograms rather than rectangles.

4 Conclusions In this work, we attempted to describe the atomic level deformations that take place when NAT, a zeolite for which negative Poisson's ratios have been experimentally measured, is mechanically deformed by applying mechanical stresses in the (001) plane. We have shown that irrespective of the force-field used, the behaviour of this zeolite in the (001) plane is describable by a 2D model involving 'rotating semi-rigid quadrilaterals', and we have shown that existing 2D models described by Grima et al. [44] and Williams et al. [55] can provide a qualitative description of some (but not all) of the aspects of the behaviour of NAT.

We show that both models need to be further improved, for example, by extending the model by Grima et al. [44] to allow for changes in lengths of the diagonals (thus permitting the quadrilaterals to become parallelograms) whilst the model of Williams et al. needs to be extended to permit the modelling of systems where not all the parallelograms in the system remain congruent to each other.

Before we conclude, it is important to point out that NAT is in reality a 3D system with a framework made from AlO_4 and SiO_4 tetrahedra. Thus, any projected deformations in the (001) plane that are being described by the 2D models of Grima et al. [44] and Williams et al. [55] are necessarily accompanied in changes in the shape, size and/or orientations of these tetrahedra. Nevertheless, given that 2D models are characterised by much less complexity than 3D models based on tetrahedra, we are confident that the work presented here will provide an impetus to researchers working in this field to further develop these existent 2D models to produce improved models which can represent the complex behaviour of NAT more accurately.

Acknowledgement The support of MCST through their National RTDI funding programme is gratefully acknowledged.

References

[1] K. E. Evans, M. A. Nkansah, I. J. Hutchinson, and S. C. Rogers, Nature **353**, 124 (1991).
[2] K. W. Wojciechowski, A. Alderson, K. L. Alderson, B. Maruszewski, and F. Scarpa, phys. stat. sol. (b) **244**, 813 (2007).
[3] L. J. Gibson, M. F. Ashby, G. S. Schajer, and C. I. Robertson, Proc. R. Soc. Lond. A **382**, 25 (1982).
[4] R. F. Almgren, J. Elast. **15**, 427 (1985).
[5] D. Prall and R. S. Lakes, Int. J. Mech. Sci. **39**, 305 (1997).
[6] A. Spadoni, M. Ruzzene, and F. Scarpa, phys. stat. sol. (b) **242**, 695 (2005).
[7] K. W. Wojciechowski, Mol. Phys. **61**, 1247 (1987).
[8] K. W. Wojciechowski and A. C. Branka, Phys. Rev. A **40**, 7222 (1989).
[9] K. W. Wojciechowski, J. Phys. A, Math. Gen. **36**, 11765 (2003).
[10] R. S. Lakes, Science **235**, 1038 (1987).
[11] K. E. Evans, M. A. Nkansah, and I. J. Hutchinson, Acta Metall. Mater. **2**, 1289 (1994).
[12] J. B. Choi and R. S. Lakes, J. Compos. Mater. **29**, 113 (1995).
[13] N. Chan and K. E. Evans, J. Cell. Plast. **34**, 231 (1998).
[14] C. W. Smith, J. N. Grima, and K. E. Evans, Acta Mater. **48**, 4349 (2000).
[15] J. N. Grima, A. Alderson, and K. E. Evans, J. Phys. Soc. Jpn. **74**, 1341 (2005).
[16] K. E. Evans and B. D. Caddock, J. Phys. D, Appl. Phys. **22**, 1883 (1989).
[17] A. Alderson and K. E. Evans, J. Mater. Sci. **30**, 3319 (1995).
[18] A. Alderson and K. E. Evans, J. Mater. Sci. **32**, 2797 (1997).
[19] R. H. Baughman and D. S. Galvao, Nature **365**, 635 (1993).
[20] C. B. He, P. W. Liu, and A. C. Griffin, Macromolecules **31**, 3145 (1998).
[21] J. N. Grima and K. E. Evans, Chem. Commun. 1531 (2000).
[22] J. N. Grima, J. J. Williams, and K. E. Evans, Chem. Commun. 4065 (2005).
[23] G. Y. Wei, phys. stat. sol. (b) **242**, 742 (2005).
[24] R. H. Baughman, J. M. Shacklette, A. A. Zakhidov, and S. Stafstrom, Nature **392**, 362 (1998).
[25] A. Yeganeh-Haeri, D. J. Weidner, and D. J. Parise, Science **257**, 650 (1992).
[26] N. R. Keskar and J. R. Chelikowsky, Phys. Rev. B **46**, 1 (1992).
[27] H. Kimizuka, H. Kaburaki, and Y. Kogure, Phys. Rev. Lett. **84**, 5548 (2000).
[28] A. Alderson and K. E. Evans, Phys. Rev. Lett. **89**, 225503 (2002).
[29] H. Kimizuka, H. Kaburaki, and Y. Kogure, Phys. Rev. B **67**, 024105 (2003).
[30] A. Alderson, K. L. Alderson, K. E. Evans, J. N. Grima, and M. Williams, J. Met. Nano. Mater. **23**, 55 (2004).
[31] A. Alderson, K. L. Alderson, K. E. Evans, J. N. Grima, M. Williams, and P. J. Davies, phys. stat. sol. (b) **242**, 499 (2005).
[32] J. N. Grima, R. Gatt, A. Alderson, and K. E. Evans, J. Mater. Chem. **15**, 4003 (2005).
[33] J. N. Grima, R. Gatt, A. Alderson, and K. E. Evans, Mater. Sci. Eng. A **423**, 219 (2006).
[34] J. N. Grima, R. Jackson, A. Alderson, and K. E. Evans, Adv. Mater. **12**, 1912 (2000).
J. N. Grima, A. Alderson, and K. E. Evans, Zeolites with negative Poisson's ratios, Paper presented at the RSC 4th International Materials Conference (MC4), Dublin, Ireland, P81, July 1999.
[35] J. N. Grima, Ph.D. thesis, University of Exeter, Exeter, UK (2000).
[36] K. W. Wojciechowski, J. Phys. Soc. Jpn. **72**, 1819 (2003).
[37] H. Kimizuka, S. Ogata, and Y. Shibutani, phys. stat. sol. (b) **244**, 900 (2007).
[38] K. V. Tretiakov and K. Wojciechowski, phys. stat. sol. (b) **244**, 1038 (2007).
[39] J. N. Grima and K. E. Evans, J. Mater. Sci. **4**, 3193 (2006).

[40] J. N. Grima and K. E. Evans, J. Mater. Sci. Lett. **19**, 1563 (2000).
[41] Y. Ishibashi and M. J. Iwata, J. Phys. Soc. Jpn. **69**, 2702 (2000).
[42] A. Alderson, K. L. Alderson, K. E. Evans, J. N. Grima, M. R. Williams, and P. J. Davies, Comput. Methods Sci. Technol. **10**, 117 (2004).
[43] J. N. Grima, A. Alderson, and K. E. Evans, phys. stat. sol. (b) **242**, 561 (2005).
[44] J. N. Grima, V. Zammit, R. Gatt, A. Alderson, and K. E. Evans, phys. stat. sol. (b) **244**, 866 (2007).
[45] C. Sanchez-Valle, S. V. Sinogeikin, Z. A. D. Lethbridge, R. I. Walton, C. W. Smith, K. E. Evans, and J. D. Bass, J. Appl. Phys. **98**, 053508 (2005).
[46] J. N. Grima, R. Gatt, V. Zammit, J. J. Williams, K. E. Evans, A. Alderson, and R. I. Walton, J. Appl. Phys. **101**, 086102 (2007).
[47] J. N. Grima, R. Gatt, A. Alderson, and K. E. Evans, J. Phys. Soc. Jpn. **74**, 2866 (2005).
[48] F. Nye, Physical Properties of Crystals (Clarendon Press, Oxford, 1957).
[49] E. de Vos Burchart, Studies on Zeolites, Molecular Mechanics, Framework Stability, and Crystal Growth, Ph.D. thesis, Technische Universiteit Delft (1992).
[50] A. K. Rappe, C. J. Casewit, K. S. Colwell, W. A. Goddard, and W. M. Skiff, J. Am. Chem. Soc. **114**, 10024 (1992).
[51] P. P. Ewald, Ann. Phys. (Leipzig) **64**, 253, (1921).
[52] P. Wagner, O. Terasaki, S. Ritsch, J. Geraldo Nery, S. I. Zones, M. E. Davis, and K. Hiraga, J. Phys. Chem. B **103**, 8245 (1999).
[53] A. T. Hugler, E. Huler, and S. Lifson, J. Am. Chem. Soc. **96**, 5319 (1974).
[54] E. de Vos Burchart, V. A. Verheij, H. Vanbekkum, and B. Vandegraaf, Zeolites **12**, 183 (1992).
[55] J. J. Williams, C. W. Smith, K. E. Evans, Z. A. D. Lethbridge, and R. I. Walton, Chem. Mater. **19**, 2423 (2007).
[56] W. M. Meier, Z. Kristallogr. **113**, 430 (1960).
[57] J. N. Grima, R. Gatt, A. Alderson, and K. E. Evans, J. Phys. Soc. Jpn. **74**, 2866 (2005).
[58] V. Zammit, MSc Dissertation, University of Malta (2008).

